Geophysical Journal International

Geophys. J. Int. (2009) **179,** 1757–1771 doi: 10.1111/j.1365-246X.2009.04374.x

Ground motion and macroseismic intensities of a seismic event related to geothermal reservoir stimulation below the city of Basel—observations and modelling

Johannes Ripperger, Philipp Kästli, Donat Fäh and Domenico Giardini

Swiss Seismological Service, ETH Zurich, Institute of Geophysics, Schafmattstr. 30, 8093 *Zurich, Switzerland. E-mail: jripperger@web.de*

Accepted 2009 August 28. Received 2009 August 27; in original form 2008 August 27

SUMMARY

To stimulate a geothermal reservoir below the city of Basel, Switzerland, fluid was injected in December 2006 at high pressure into a 5 km deep borehole. This stimulation led to an increase in local seismicity with the largest seismic event ($M_L = 3.4$) occurring on 2006 December 8. The event was widely felt by the local population, slight non-structural damage to buildings was reported and ultimately this event was the cause to put the geothermal project on hold. In this study, we present recorded ground motion and determinations of macroseismic intensity of the M_L 3.4 event as well as simulations of seismic wave propagation and a model to predict macroseismic intensities. As the two models are based on different simplifying assumptions and different underlying physical processes, the predicted intensity distributions exhibit differences in their details. However, the first-order characteristics of the observed macroseismic intensity distribution are well matched. Based on this result, we compute intensities also for hypothetical scenarios of earthquakes with larger magnitudes.

Key words: Earthquake ground motions; Site effects; Computational seismology; Wave propagation.

1 INTRODUCTION

In 1998 the 'Deep Heat Mining' (DHM) project was initiated by a private industry consortium (Geopower Basel AG) with the goal to exploit the geothermal potential of the crystalline rocks below the city of Basel, Switzerland. The technique to be applied in the DHM project for production of heat and electric energy is commonly termed the 'hot dry rock' method. It requires the generation of a geothermal reservoir, that is a connected network of cracks and fissures through which fluid can circulate. This creation of a reservoir is achieved by injecting fluid under high pressure into a borehole, a process often termed hydraulic stimulation.

After successful completion of the first main well Basel-1 in October 2006, the hydraulic stimulation phase began on 2006 December 2. To monitor the increased seismic activity that always accompanies the stimulation phase, a very sensitive network of seismic borehole-sensors had been installed by the private company in charge of the project, Geothermal Explorers Ltd. (GEL). In fact, the shape of the zone of micro-seismic activity surrounding the stimulation borehole gives important indications on the development of the geothermal reservoir and is therefore an integral part of the methodology. Since it was known that the stimulation could also induce or trigger larger events (e.g. Baisch *et al.* 2006; Charléty *et al.* 2007) that might be felt by the local population or could even lead to building damage, an alarm system was implemented based on thresholds in magnitude and peak ground velocity (PGV) of the occurring earthquakes that would lead to immediate reduction of the injection rate or even a stopping of the stimulation if the corresponding thresholds would be reached. This threshold alarm system was developed along the lines of a similar procedure implemented for a geothermal project in El Salvador (Bommer *et al.* 2006). The Swiss Seismological Service ('Schweizerischer Erdbeben Dienst', SED) was responsible for the actual magnitude and PGV determination that served as input to trigger the alarm levels and for information of the public. The SED also deployed six temporary strong-motion instruments in the area to complement the permanent network.

Soon after the injection started, significant seismic activity was detected and on 2006 December 8, an earthquake with local magnitude $M_L = 2.7$ occurred, which prompted GEL to reduce the injection rate and then to stop the injection completely. Later on the same day a seismic event took place that was widely felt in the area of Basel and caused slight non-structural damage (e.g. hairline cracks in walls or minor pieces of plaster falling down) to buildings (e.g. Aegeter & Bosshardt 2007). This event unsettled the local population and received nationwide and also international media attention. Its hypocenter was determined to be close to the injection well with a focal depth of roughly 5 km. The event was assigned a local magnitude $M_L = 3.4$ by the SED and led to an immediate halt of the geothermal experiment. Since then, the seismic activity slowly decayed. However, several $M_L > 3$ events in the following months continued to disconcert the local population. At present, the DHM project is still on hold and awaits an independent risk-analysis study to be completed, before public authorities will decide on a continuation of the project. Regarding the threshold alarm system, it has

become clear from the Basel project, as well as from other similar projects, that such a system does not provide a definitive solution to the hazard associated with the seismicity induced by geothermal reservoir stimulations. As also pointed out by Majer *et al.* (2007), the largest events seem to occur after pumping has ceased and therefore to rely on a system that provides alerts as to when pumping should be suspended does not provide a risk management solution.

To date, several thousand damage claims related to the M_L 3.4 event have been documented (e.g. Aegeter & Bosshardt 2007) and the total amount of compensation payments made by insurance companies and Geopower Basel AG is estimated to be in the range of several million Euros. The seismic sequence, and in particular the largest event, bears great importance in terms of public perception of the DHM project in Basel and geothermal projects in general and may have strong influence on future political decisions regarding such projects. In particular, the regulatory requirements for careful evaluation of the seismic hazard associated with geothermal reservoir stimulation are expected to become more restrictive for any future project. It therefore is timely to investigate the Basel seismic sequence and in particular the main shock (M_L 3.4 event of 2006 December 8, origin time: 16:48:39.172 UTC, hypocenter location: 611643/270420 in Swiss coordinates, depth below sea level: 4701 m) and its impact in detail. The present study focuses on this event and utilizes empirically derived macroseismic relations along with numerical simulations of seismic wave propagation to model the recorded ground motions and its effects. This approach ultimately aims at providing answers to the following questions: Which models and input parameters are needed to reproduce the observed ground motion and its effects by macroseismic and/or wave-propagation models?Was there something unusual about the M_L 3.4 event or could its effects have been predicted with reasonable accuracy with the information available before the start of the reservoir stimulation?

The study is organized as follows: First of all, an overview of the observed data is given in Section 2. Sections 3 and 4 constitute the main part of this paper and describe in detail the macroseismic and wave-propagation modelling, respectively. Both modelling approaches are compared and discussed in the subsequent Section 5. In Section 6, scenario calculations for hypothetical larger events in the Basel area are presented, before Section 7 completes the paper with general conclusions.

2 OBSERVATIONS OF THE M_L 3.4 2006 DECEMBER 8, EVENT

2.1 Instrumental data

The seismic waves generated by the M_L 3.4 event were recorded by a large number of stations (Fig. 1). In the present analysis we use 17 of the permanent strong-motion stations of the SED plus 4 permanent stations operated by the Landeserdbebendienst Baden-Württemberg (LED) in the area of Basel (Table 1). In addition, six temporary strong-motion recorders had been placed by the SED within and around the city of Basel during the main stimulation phase and for some weeks to months afterwards (Table 1). Some of these temporary stations had been positioned specifically at places where amplification of ground motion was expected from knowledge of the geological site conditions, which feature a loess layer of few meters thickness, unconsolidated alluvial deposits or landslide material at the top. In the Rhine Graben, the unconsolidated sediments have a thickness of 5 to 50 m and are composed of Pleistocene and Holocene sandy gravels. They were deposited by the River Rhine and its tributaries. These sediments are above Tertiary sediments that might have average shear-wave velocities as low as 500–600 m s^{-1} (Fäh & Huggenberger 2006). On the hill tops large areas are covered by Loess layers of up to 15 m thickness. To the east, on the shoulder of the Rhine-Graben, the Mesozoic sediments of the Tabular Jura are covered directly by 5 to 50 m thick Pleistocene and Holocene colluvial deposits and isolated patches of Pleistocene gravels. In the Rhine valley up to 45 m of mostly sandy Rhine gravels overlay Mesozoic bedrock. We also include seven temporary stations installed by the LED. The event was recorded by six borehole sensors surrounding the injection well at depths between 300 m and 2700 m which were operated by GEL. These borehole stations have been utilized for the precise determination of the event locations but are not used in this study.

Seismograms at the strong-motion stations (Fig. 2) have been converted from the original accelerometer recordings to ground velocity by the following processing steps: After removing the mean the acceleration time histories have been filtered using a fourth-order Butterworth highpass filter with a cutoff frequency of 0.2 Hz. Subsequently the traces have been integrated using a cumulative trapezoidal integration scheme. At all stations the arrival of the direct *S* wave is the most prominent feature in the seismic waveforms and is responsible for the peak ground velocity value.

2.2 Macroseismic data

The macroseismic data collected after the main shock represents a good opportunity to check the performance of Swiss intensity-attenuation models. The SED collected roughly 850 interpretable reports on the main event, applying its standard procedures for the collection of macroseismic data:

(1) Around 750 reports were spontaneous contributions mostly using the responding questionnaire on the website of the SED (http://www.seismo.ethz.ch/info/).

(2) The remaining 100 reports were reactions to an email request of the SED to 280 constant contact persons in the presumed felt area and adjacent regions (Jura and northern Switzerland). The contact persons were asked to report whether they have felt the event or not, and what there observations were. The response was again collected using the same web questionnaire.

The apparently low response to the email enquiry is due to the fact that many of the contact persons, especially from Basel city, had already spontaneously reported the earthquake when the email request was sent out ∼3 hr after the event. Analysis of the questionnaires for intensity assessment was done based on the EMS-98 scale (Grünthal 1998). In a first step, a computer code interprets the answers to precise questions only, using statistical procedures and exclusion criteria. In a second step, all intensity assignments were checked manually, also including freetext observations delivered with the questionnaires. Macroseismic intensities could be assigned to 92 settlements or (in the case of Basel city) zip-code areas. Of these, 41 are considered to be of medium or good quality, relying on 5 or more independent eyewitnesses each. Counterchecks showed no difference between intensities estimated from spontaneous reports and intensities derived from requested ones of the same area, as long as the intensities are in the range of IV to V. From places with observed intensity III, the number of spontaneous reports is considerably lower. The effects described, however, do not notably differ from those described in requested reports. Reported intensities in the range I to II are usually badly constrained. The

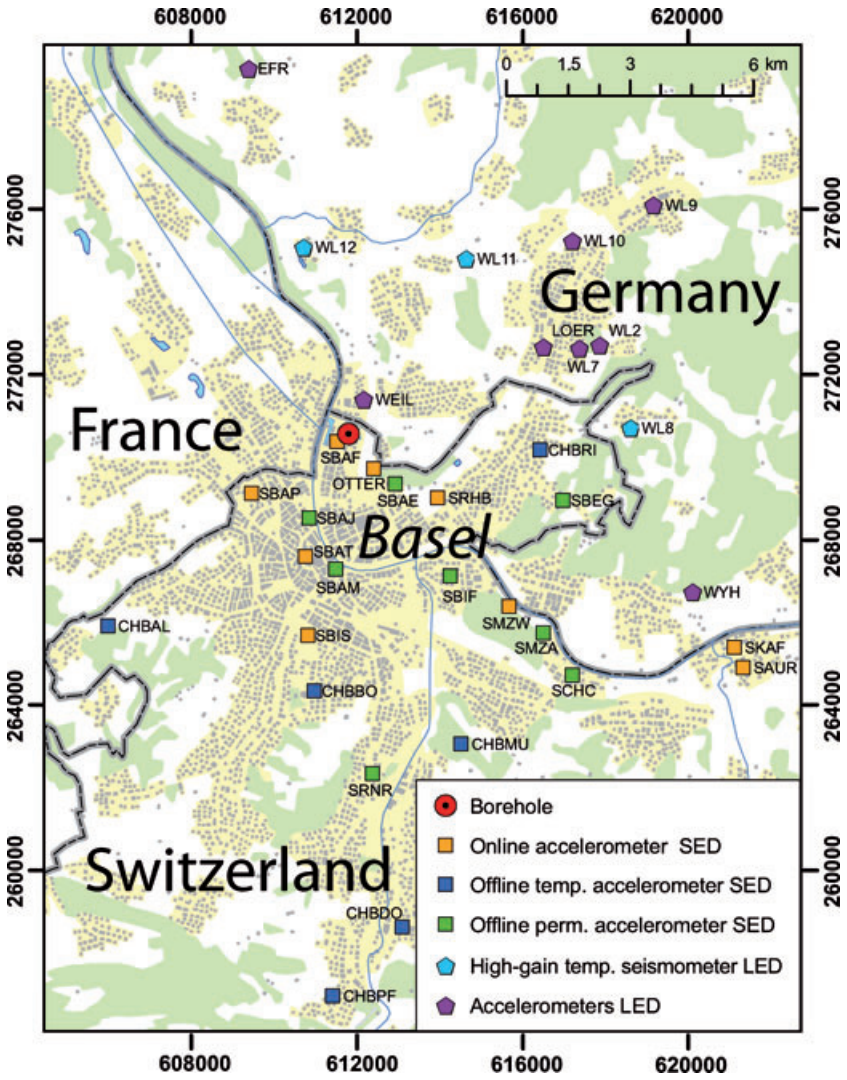

Figure 1. Map showing the seismic stations used in this study.

number of observations available from such places is often not sufficient to distinguish between intensity I, II and III. At Intensity II, up to 1 per cent of the population is supposed to feel an earthquake. This percentage would require up to 200–300 interrogated people per settlement to be reliably determined. However, already the detection of an intensity III (event felt by 10–15 per cent of the population) from 10 or less reports widely relies on assumptions.

Of the 865 observations, 40 or 4.6 per cent reported non-structural damage to buildings (haircracks in walls 31 times, minor pieces of plaster falling down in 9 cases). Within the area of Basel City, 23 reports out of 403 (5.7 per cent) mentioned such damage. Several days after the event, Geopower Basel launched a request for damage claims. This request resulted in a data set of more than 2000 building-damage reports of which ∼900 originated from within the city of Basel (∼4.7 per cent of the building stock; preliminary data). However, these reports were not included in the intensity assessment, as they were not complemented with reports of human perception and effects to objects. Including them would emphasize a special type of effects in the data set and thus derogate the representativity of the overall macroseismic description of the event.

Although there is no direct relationship between macroseismic intensity and any ground-motion parameter, different relationships have been derived for comparison of intensity to peak ground acceleration PGA (e.g. Murphy & O'Brien 1977), peak ground velocity PGV (e.g. Atkinson & Kaka 2007), spectral values (e.g. Ebel & Wald 2003), Housner intensity (Housner 1952) and Arias intensity (Margottini *et al.* 1992). Recent studies found that PGV is a better proxy for intensity than PGA, especially at higher intensities (e.g. Wald *et al.* 1999; Kästli & Fäh 2006). However, the relationship between intensity and PGV may depend on many additional factors, such as magnitude, epicentral distance, frequency content, etc. To check whether the typical regional relationships between ground motion and intensity apply also for this deep heat mining event, we calculated instrumental intensity values from PGV measurements at seismic stations using the empirical relationship of Kästli & Fäh (2006). This stepwise conversion formula is based on 210 sets of intensity assignments (ranging from Intensity I to Intensity VII) compared to PGV measurements of nearby seismic stations, from events between magnitude $M_W = 2.0\ldots6.7$ in Switzerland and adjacent countries.

The display of macroseismic intensities in Fig. 3 is restricted to intensity data-points (IDP) of medium or good quality (based on 5 or more independent reports). A consistency check revealed that in more than 80 per cent of the cases these intensity assignments

Table 1. List of strong-motion stations used in this study.

Name	CH E	CH N	CH Z	Type	Operator	Distance (km)	PGV (cm s^{-1})
CHBAL	605977	265874	334	temporary	SED	7.3	0.276
CHBBO	610990	264286	353	temporary	SED	6.2	0.751
CHBDO	613119	258542	324	temporary	SED	12.0	0.043
CHBMU	614533	263012	332	temporary	SED	8.0	0.078
CHBPF	611434	256863	351	temporary	SED	13.6	0.195
CHBRI	616471	270142	291	temporary	SED	4.8	1.017
EFR	609393	279418	270	Permanent	LED	9.3	–
LOER	616535	272651	270	Permanent	LED	5.4	0.317
OTTER	612428	269691	250	Permanent	SED	1.1	1.177
SAUR	621398	264835	290	Permanent	SED	11.2	0.183
SBAE	612948	269314	254	Permanent	SED	1.7	0.572
SBAF	611539	270345	248	Permanent	SED	0.1	0.488
SBAJ	610857	268476	250	Permanent	SED	2.1	1.389
SBAM	611514	267243	277	Permanent	SED	3.2	0.376
SBAP	609464	269085	263	Permanent	SED	2.6	0.510
SBAT	610769	267553	260	Permanent	SED	3.0	0.723
SBEG	617019	268924	370	Permanent	SED	5.6	0.235
SBIF	614292	267082	255	Permanent	SED	4.3	0.300
SBIS	610832	265629	315	Permanent	SED	4.9	0.597
SCHC	617250	264666	270	Permanent	SED	8.0	0.153
SKAF	621178	265335	270	Permanent	SED	10.8	0.100
SMZA	616539	265687	254	Permanent	SED	6.8	0.205
SMZW	615709	266341	272	Permanent	SED	5.8	0.387
SRHB	613979	268972	260	Permanent	SED	2.7	0.303
SRNR	612398	262263	293	Permanent	SED	8.2	0.188
WEIL	612189	271380	240	Permanent	LED	1.1	0.306
WL2	617913	272693	390	Temporary	LED	6.7	0.310
WL7	617425	272617	330	Temporary	LED	6.2	0.678
WL8	618659	270675	360	Temporary	LED	7.0	0.323
WL9	619218	276106	310	Temporary	LED	9.5	–
WL10	617255	275229	240	Temporary	LED	7.4	–
WL11	614662	274796	420	Temporary	LED	5.3	–
WL12	610727	275066	240	Temporary	LED	4.7	–
WYH	620165	266696	350	Permanent	LED	9.3	0.146

CH E / CH N / CH Z: East/North/Elevation above sea level, all values are given in meters in the Swiss coordinate system.
Distance = epicentral distance.
PGV = max($\sqrt{v_x^2 + v_y^2}$), requiring both horizontal velocity time histories v_x and v_y. Because the full waveforms were not available for some of the LED stations, no PGV value is given for these stations.

do not depend on the person carrying out the analysis (Kästli *et al.* 2006). Although macroseismic and instrumental intensity have different reference areas (macroseismic intensity describes the effects of ground motion averaged across the whole settled area of a municipality, while instrumental intensity only describes the specific site of the instrument), the agreement is fairly good, and mostly within the standard error of the conversion formula (∼1 intensity unit, varying over the scale).

3 MACROSEISMIC MODELLING

Observed intensities may be compared to a modelled intensity map. The used model is based on a point source with regular energy radiation. A moment magnitude of $M_W = 3.0$ is assumed, as this value has been determined by a detailed spectral analysis of the displacement time-series (Bethmann *et al.* 2007). First of all a grid of expected intensities is derived for soil class B (stiff sediments) of the SIA (Schweizerischer Ingenieur- und Architektenverband, SIA (2003)) and the Swiss macroseismic attenuation relation of Fäh *et al.* (2003a) for shallow foreland events. To this value, an additive correction factor is applied accounting for soil-specific amplification for each soil class represented in the geological and tectonic maps of Switzerland 1:500 000 (BfL 2006a,b). Correction factors are derived from mean residuals between observed intensity and attenuation-based predictions, based on a pool of all macroseismic intensity assignments available for Swiss earthquakes since 1850.

An intensity model was calculated for an area of 60 × 60 km, covering the region between Biel, Sursee, Altkirch (France), and Schopfheim (Germany). Attenuation effects were discretized with a grid resolution of 100 m as well as site amplification effects according to the geological base map with a resolution of 1:500 000. The epicentral area of the intensity model makes up the background color in Fig. 3.

For the quantitative assessment of the model quality, only data from a circle with a radius up to 20 km around the epicenter was used. This circle corresponds roughly to the area where intensities of III+ are expected. The number of reports per locality was too low to assess intensities II within a reasonable confidence level. To compare the model prediction with observed intensities, mean expected

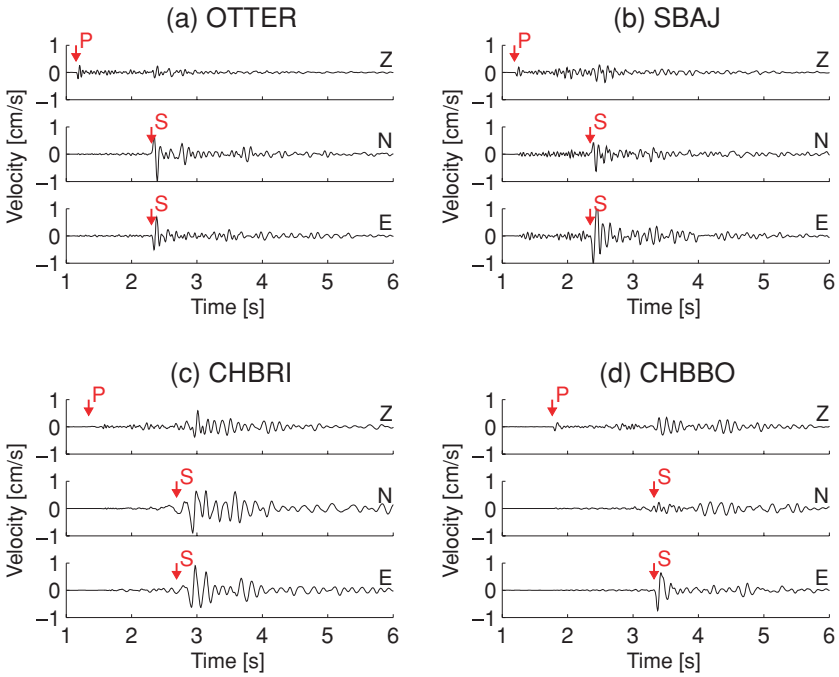

Figure 2. Example time histories of ground motion recorded during the M_L 3.4 event of 2006 December 8. The waveforms have been converted to ground velocity from the original accelerogram recordings. (a) Seismograms at station OTTER close to the epicenter (∼1100 m epicentral distance). (b) Seismograms at station SBAJ at ∼2100 m epicentral distance. (c) Seismograms at the temporary station CHBRI, which was located on unconsolidated sediments at a distance of ∼4800 m from the epicenter. (d) Seismograms at the temporary station CHBBO located on unconsolidated sediments at ∼6200 m epicentral distance.

model-intensities were calculated in circles with 100 m diameter around the sites of the instruments, and 500 m diameter around IDP coordinates. The larger area for macroseismic IDPs is chosen because places from which reports are coming may be distributed over a whole settlement or zip-code area. Instrumental measurements are point measurements, and the assumed positioning uncertainty of the geotechnical map defines the 100 m radius at instrument locations. To properly interpret the results of this comparison, it is important to keep in mind, that only integer values of intensity have a well defined meaning. In contrast, the decimal fractions of intensity, which arise from the treatment of intensity as a continuous variable in the prediction equations, have no physically interpretable meaning.

The results of the comparison for the IDP's (circles in Fig. 3) are as follows (Fig. 4):

(1) 27 of 38 macroseismic IDPs (71 per cent) are predicted correctly by the model.
(2) 11 macroseismic IDPs (29 per cent) are predicted with an error of one intensity unit.
(3) No macroseismic IDP is predicted with an error of two or more intensity units.
(4) In the mean, predicted intensities are nearly identical (0.02 units higher) to the observed ones.

Within an epicentral distance of 20 km, where reliable macroseismic data is available, there is no dependence of the IDP residuals on distance. The near-field part of the macroseismic attenuation relation predicts the observations well. The clear split of the residuals in two groups (one >0 and the other <0) is typical for a situation of an intensity at the edge of two classes (here IV–V), when intensity assignments done in integers are compared to a model using a continuous scale. This effect disappears in the intensity IV area between 7 and 15 km epicentral distance. Also instrumentally derived intensities are similar to the model on average (model deviation: +0.19 intensity units). However, with differences of up to 2.4 units between modelled and observed intensities, the scatter is much higher. This difference may have several reasons. Besides the additional uncertainty introduced by the PGV-to-intensity conversion, the installation conditions for the instruments are heterogeneous: While strong-motion stations in Basel are deployed in places representative for conditions of the built environment, other station sites are selected for lowest possible noise level, preferably on bedrock. Station WYH for example has a model deviation of +1.4 intensity units, and is located on hard bedrock. We therefore might expect low shaking. The site amplification map does not resolve the bedrock condition at such sites. Another important reason for the differences at some sites is the effect of the source radiation, for example with low amplitudes in the south–east of Basel (see also discussion in Section 5). This effect likely is responsible for the largest model residual of +2.4 intensity units at station CHBMU, which is located close to a minimum of the *S*-wave radiation pattern. It therefore experienced lower shaking than predicted by the macroseismic model, which does not include information on the source radiation.

4 GROUND-MOTION MODELLING

4.1 General approach and methods

The general approach of ground-motion modelling taken in this study was to start with simple 1-D models before moving on to the full 3-D waveform modelling. The 1-D simulations are useful for efficiently estimating the influence of the various ingredients of the simulations on the resulting seismograms. At the same time they provide a reference solution to which the 3-D simulation results can be compared.

The 1-D simulations were performed with the wavenumber-integration codes included in the software package 'Computer

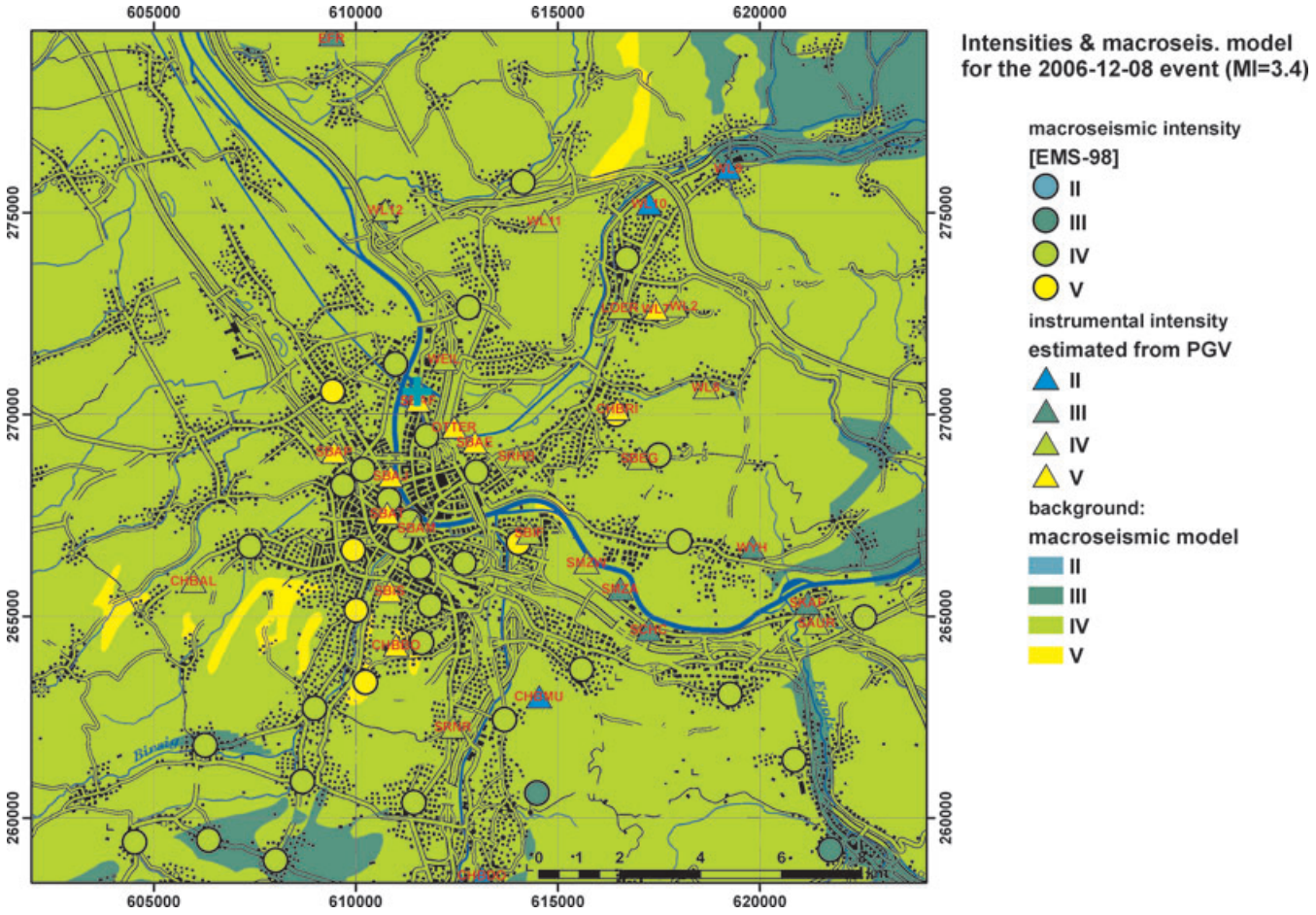

Figure 3. Map of the epicentral area providing a visual comparison of the intensities predicted by the macroseismic model (background colors) with the observed macroseismic intensities (circles) and the intensities derived from instrumental PGV (triangles).

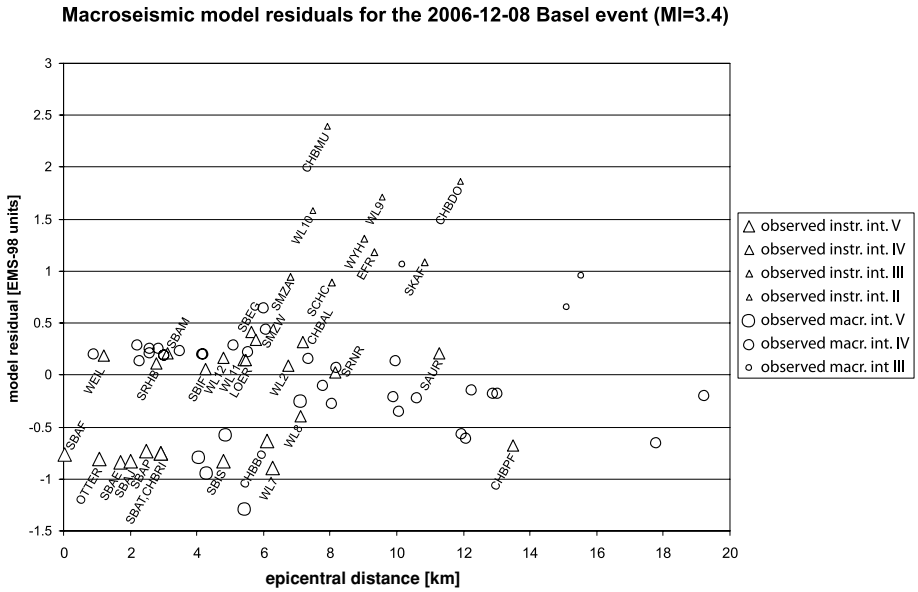

Figure 4. Predicted minus observed intensity for macroseismic and instrumental intensities. A scatter of 0.5 intensity units is due to the fact that a residual results from comparing the continuous values of predicted 'pseudo-intensity' with the integer values of observed intensity.

Programs in Seismology' (Herrmann 2004). The simulations of seismic wave propagation in 3-D were carried out using the finite-difference code AWM (for 'Anelastic Wave Model') developed by Kim Olsen and Co-workers (Olsen 1994; Olsen *et al.* 2003).

4.2 Available structural models

Several models of the seismic velocity and density structure below the city of Basel have been developed and have been used for different purposes. In this study, the 1-D model presented by Fäh *et al.* (2003b) for a molasse bedrock (Table 2) serves as a reference model in both 1-D and 3-D simulations. This regional 1-D model (hereinafter referred to as '1-D reference model') has been constructed using information from seismic reflection and refraction measurements and was developed for regional moment-tensor inversion (Campus & Fäh 1997).

Furthermore, 1-D models of the shallow seismic velocity and density structure at selected locations in the area of Basel (including all sites where strong-motion instruments are installed) had been obtained by inverting array measurements of ambient seismic noise (Fäh & Huggenberger 2006). These 1-D models (hereinafter referred to as 'local 1-D models') are used in 1-D simulations in the present study to compute synthetic seismograms at the locations of the strong-motion stations.

Finally, this study makes use of a 3-D structural model of the visco-elastic medium properties in the Basel region. This model has been constructed in 2001 at the ETH Zurich, based on the 3-D geological model made available at that time (Zechner *et al.* 2001) by the Kantonsgeologie of Basel Stadt. Note, that the 3-D geological model has been updated more recently (Spottke *et al.* 2005). The geophysical parameters have been derived from compiled borehole data as well as from measurements of the fundamental frequency of resonance of the soils and *S*-wave velocities at 6 locations (Kind 2002, and references therein). This geophysical 3-D model has been used in slightly modified form by Opršal *et al.* (2005) for modelling the strong ground motion in Basel for different earthquake scenarios including the historical event of 1356.

The area covered by the model has extensions of 18 km in East-West direction and 20 km in North–South direction with the lower left corner at 602 000/255 000 in the Swiss coordinate system. The model itself consists of six main interfaces plus the topography, resulting in seven main layers. Three of these seven layers between the main interfaces are further subdivided into mutually parallel sublayers which follow the overlying free surface topography. The topography and the main interfaces are provided on a rectangular grid with 50 m spacing in both directions. Each layer or sub-layer is characterized by five independent parameters: *P*- and *S*-wave velocity, density and quality factors for *P*- and *S* waves (Table 3).

Note, that the geometry of all interfaces was modified to level the topography because the 3-D code used in this study assumes a

Table 2. Regional bedrock 1-D reference model.

Depth (km)	Thickness (m)	V_P ($m\,s^{-1}$)	V_S ($m\,s^{-1}$)	Density ($kg\,m^{-3}$)	Q_P (−)	Q_S (−)
0.000	10	2400	1200	2300	200	100
0.010	10	2800	1400	2300	200	100
0.020	10	3150	1800	2300	200	100
0.030	110	3200	1850	2400	200	100
0.140	120	3300	1910	2400	200	100
0.260	120	3400	1970	2400	200	100
0.380	120	3800	2190	2400	200	100
0.500	200	4200	2420	2500	250	100
0.700	200	4300	2480	2500	250	100
0.900	200	4650	2680	2500	250	100
1.100	200	4650	2680	2500	250	100
1.300	200	5000	2890	2600	250	100
1.500	200	5000	2890	2600	250	100
1.700	100	5000	2890	2600	250	100
1.800	200	5450	3150	2600	250	100
2.000	200	5450	3150	2600	250	100
2.200	100	5450	3150	2600	250	100
2.300	200	5900	3410	2600	250	100
2.500	200	5900	3410	2600	250	100
2.700	500	6100	3520	2600	250	100
3.200	500	6100	3520	2600	250	100
3.700	1000	6100	3540	2850	500	200
4.700	1000	6140	3560	2850	562.5	225
5.700	1000	6180	3580	2850	562.5	225
6.700	1000	6220	3600	2850	562.5	225
7.700	1000	6260	3620	2850	562.5	225
8.700	1000	6300	3640	2850	562.5	225
>9.700	–	6320	3652	2850	562.5	225

Table 3. Geophysical parameters of the layers in the 3-D model.

Layer	Depth range (m)	V_P ($m\,s^{-1}$)	V_S ($m\,s^{-1}$)	Density (kg/m^3)	Q_P (−)	Q_S (−)
1	–	900	450	1850	30	15
2	0–25	1800	650	1850	50	25
2	25–50	1800	650	2000	50	25
2	50–75	1800	850	2000	50	25
2	75–100	1800	925	2000	50	25
2	100–150	1800	1000	2000	50	25
2	150–200	1800	1025	2000	50	25
2	200–250	1800	1050	2000	50	25
2	250–300	1800	1075	2000	50	25
2	300–350	1800	1100	2000	50	25
2	350–400	1800	1125	2000	50	25
2	400–450	1800	1150	2000	50	25
2	450–500	1800	1175	2000	50	25
2	500–550	1800	1200	2000	50	25
2	>550	1800	1225	2000	50	25
3	0–25	1800	575	1850	50	25
3	25–50	1800	575	2000	50	25
3	50–75	1800	675	2000	50	25
3	75–100	1800	725	2000	50	25
3	100–150	1800	775	2000	50	25
3	150–200	1800	825	2000	50	25
3	200–250	1800	850	2000	50	25
3	250–300	1800	875	2000	50	25
3	300–350	1800	900	2000	50	25
3	350–400	1800	925	2000	50	25
3	400–450	1800	950	2000	50	25
3	450–500	1800	975	2000	50	25
3	500–550	1800	1000	2000	50	25
3	>550	1800	1025	2000	50	25
4	0–25	1800	500	2000	50	25
4	25–100	1800	600	2000	50	25
4	100–200	1800	650	2000	50	25
4	200–300	1800	700	2000	50	25
4	300–400	1800	750	2000	50	25
4	400–500	1800	800	2000	50	25
4	>500	1800	850	2000	50	25
5	–	3400	2000	2500	125	50
6	–	4200	2400	2550	125	50
7	–	5200	2800	2650	125	50

planar free surface. However, as the topography in the area under consideration is not very pronounced (maximum elevation difference ∼600 m over the whole 18 km × 20 km area), the distortions of the interface geometry remain small. Hereinafter the geophysical 3-D model with leveled topography will simply be referred to as the '3-D model'.

4.3 One-dimensional modelling

4.3.1 Influence of focal mechanism

Even for well recorded events such as the M_L 3.4 event of December 2006 there remains a non-negligible uncertainty in the determination of the focal-mechanism parameters. Furthermore, for estimations of the impact of future earthquakes the exact focal mechanisms will not be known, but their approximate orientation may be anticipated from studies of the regional and local tectonic stress regimes (Kastrup *et al.* 2004; Deichmann *et al.* 2007). Therefore the influence on the peak ground motion originating from variation of the assumed focal mechanism of a simulated earthquake is investigated.

We performed 1-D simulations of the M_L 3.4 earthquake of December 2006, using the focal-mechanism parameters and the seismic moment of the most recent determination of the Swiss Seismological Service (SED 2007) of that event ($M_W = 3.0$, strike = 12°, dip = 75°, rake = −13°). Note that the approximately N-S trending nodal plane was chosen because it appears to agree well with the orientation of the general regional stress field. This choice however does not have an impact on the simulated seismograms, as the seismograms are identical for both nodal planes. In addition, variations of ±10° in the strike, dip and rake angle were considered. A total of 27 different mechanisms were computed. In this step of the analysis the 1-D reference model was used to focus on the influence of the varying focal mechanisms.

For almost all stations, the simulated peak ground velocity (PGV) values are lower than the observed ones (Fig. 5a). This discrepancy is an expected result which is due to using a regional bedrock reference-model in the simulations, while most of the stations are actually situated on unconsolidated sediments amplifying the ground shaking. We note however, that for stations, at which the 1-D reference model can be considered appropriate (e.g. stations SBEG, SKAF and WYH), the simulated PGV values match the observed ones well. The maximum variation of PGV values from the average value ranges between ±0.014 cm s^{-1} and ±0.15 cm s^{-1}. Normalized to the average PGV values, the variation ranges between ±16 per cent and ±90 per cent. For some of the sites the ground motion is very sensitive to small variations of the source mechanism (e.g. SBAF).

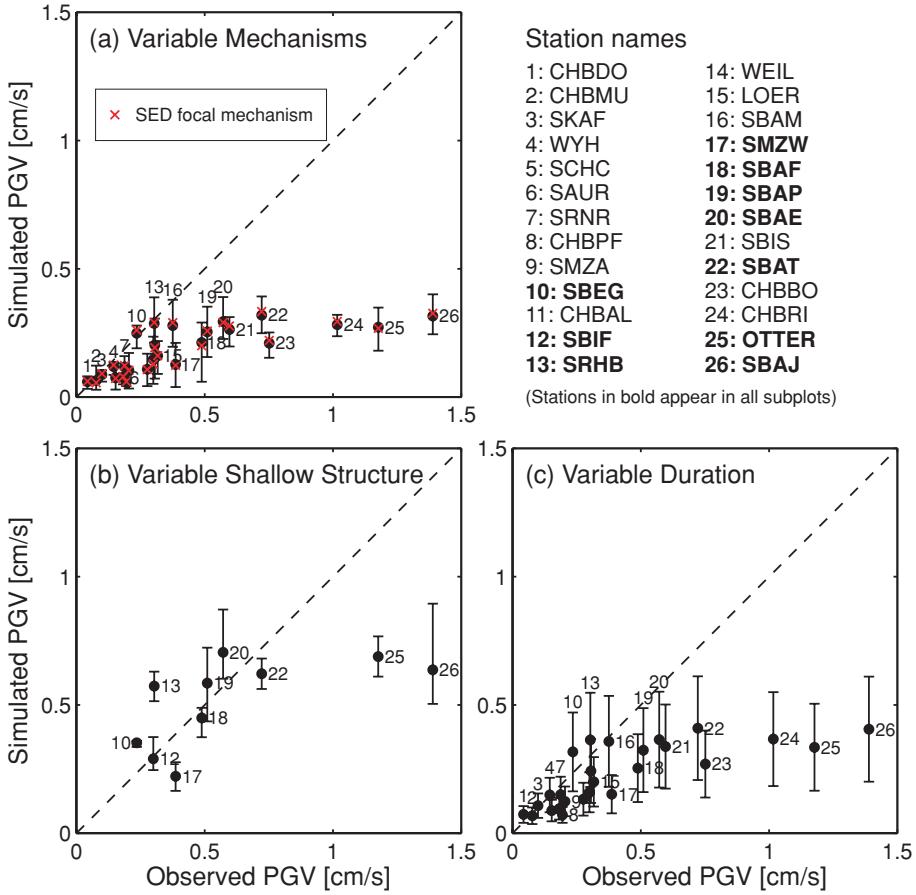

Figure 5. Peak ground velocity (PGV) values obtained by 1-D simulations using (a) the 1-D reference model and varying focal mechanisms, (b) varying structural models and (c) the 1-D reference model and varying duration of the source pulse. The errorbars in (b) span the range between the minimum and maximum PGV value obtained during the simulations for different velocity models.

4.3.2 Influence of shallow structure

For the strong-motion stations in the area of Basel detailed information on the subsurface velocity structure is available. Very recently, array measurements of ambient seismic noise have been performed at the site of each strong-motion station and these measurements have been inverted to reveal the local shear-wave velocity structure (Fäh & Huggenberger 2006; Havenith *et al.* 2007).

However, this inversion is non-unique and therefore resulted in a suite of possible local velocity structures for each station. To estimate the variation in peak ground motion that originates from this uncertainty we performed individual 1-D simulations for each of these possible local structures. These simulations were done for the subset of stations where multiple structures are available. Because the inversion is only able to well resolve the uppermost part of the velocity structure, the lower part (approximately below 100–200 m depth) was taken from the available 3-D model.

The maximum variation in PGV between the different structural models is largest at station SBAJ where it reaches 0.39 cm s^{-1} or roughly 40 per cent of the average value (Fig. 5b). Compared to the simulations using the 1-D reference model (Figs 5a and c) the simulated PGV values are higher, thus improving the fit to the observed values. However, the large PGV values observed at stations OTTER and SBAJ are still always underpredicted by the simulations. Potential reasons for this discrepancy include an incorrect representation of the source pulse duration and/or an incorrect representation of the medium attenuation in the models.

4.3.3 Influence of source time-function

A further factor that influences the peak ground motions of the simulated seismograms is the shape and duration of the assumed moment-rate function of the earthquake source. In this study a pulse with a parabolic shape is assumed for all simulations and only its duration is varied. The relative simplicity of this moment-rate function is suggested by investigations of the moment-rate function of small events (e.g. Dreger *et al.* 2007). The moment-rate function we assumed is specified as

$$\begin{aligned} m(\tau) &= \tau^2 && \text{for} \quad 0 < \tau < 1/4 \\ m(\tau) &= -\tau^2 + \tau - 1/8 && \text{for} \quad 1/4 \leq \tau < 3/4 \\ m(\tau) &= \tau^2 - 2\,\tau + 1 && \text{for} \quad 3/4 \leq \tau < 1, \end{aligned} \tag{1}$$

where τ represents time t normalized by the total duration T of the pulse. To model the M_L 3.4 earthquake of 2006 December 8, we varied the duration of the source pulse between $T = 0.08$ s and $T = 0.16$ s as this is the range of durations suggested by studies of the source duration of small earthquakes (e.g. Dreger *et al.* 2007; Kanamori & Brodsky 2004). The actual source duration of the event is estimated to be on the lower end of this range. Our calculations reveal, that in general, a shorter duration of the source pulse leads to higher peak ground velocities (Fig. 5c). When comparing Figs 5(a) and (c) we find that the peak ground motions are more sensitive to the change in duration than to the varying focal mechanisms.

4.4 3-D modelling

The propagation of seismic waves is simulated in a rectangular volume with horizontal dimensions of roughly 18 × 20 km and extending down to a depth of 10 km. Within this volume the 3-D model was discretized on a numerical grid with 25 m spacing. At the side and bottom boundaries of the grid a 10 point wide region is used for the absorbing boundary conditions to avoid reflections from the model edges. This damping region extends into the model space, leaving a 17.5 × 19.5 km area of valid simulation space extending eastwards and northwards from 602250/255250 in the Swiss coordinate system. The earthquake source is specified as a double-couple point-source with the most recent determination of seismic moment and focal mechanism by the SED (see Section 4.3.1) and the same parabolic time function of moment release as has been used for the 1-D simulations (see Section 4.3.3) with a pulse duration of $T = 0.12$ s.

Table 4. Modelling parameters of the 3-D simulations.

Parameter	Value	Unit
Grid spacing *dx*	25	m
Time step *dt*	0.002	s
Simulated time	7	s
Total grid size	720 × 800 × 400	Grid points
PML thickness	10	Grid points

PML: Perfectly Matched Layers absorbing boundary condition.

The maximum frequency up to which the 3-D simulations are valid is determined by the grid spacing, the lowest velocity present in the structural model and the required number of grid points per wavelength. Assuming that at least six points per wavelength are required, the grid spacing of 25 m and the lowest shear-wave velocity of 450 m s^{-1} yield a maximum frequency of $f_{\max} = (450\,\text{m s}^{-1})/(6 \times 25\,\text{m}) = 3$ Hz. The modelling parameters are summarized in Table 4. Each 3-D simulation required about 25 GB RAM and took approximately 4.5 hr on 32 processors of a parallel computing cluster.

4.4.1 1-D reference model

As a cross-check of the simulation setup, an initial 3-D simulation using the 1-D reference model verified that the results are identical to the ones obtained by the 1-D simulations using the same model. The horizontal PGV distribution obtained from this initial 3-D simulation visualizes the four main lobes of the radiation pattern (Fig. 6a) with the two lobes of highest PGV values located in the most densely populated areas (Schneider-Sliwa *et al.* 1999) of the Basel region.

4.4.2 3-D model

In the following we present the results of a 3-D simulation incorporating the geophysical 3-D model of the Basel region. For comparison between recorded signals and synthetic seismograms, both have been lowpass filtered using a second-order Butterworth filter with a cutoff frequency of 3 Hz. At station OTTER the timing and amplitude of the main *S*-wave arrival at roughly 2.4 s is well modelled (Fig. 7a). The fit is not as good at station CHBRI (Fig. 7b), probably because the local subsurface geology plays a more important role and is insufficiently represented in the assumed 3-D model for this temporary station. At all other stations the comparison of the filtered signals yields a similar picture: The maximum amplitude of the first *S*-wave arrival is generally well represented within a range of ±0.1 cm s^{-1} and for the majority of stations it is slightly underestimated by less than 0.05 cm s^{-1}. The worst fit in terms of the *S*-wave amplitude is obtained for stations CHBRI and SBAJ with an underestimation of ∼0.105 cm s^{-1}.

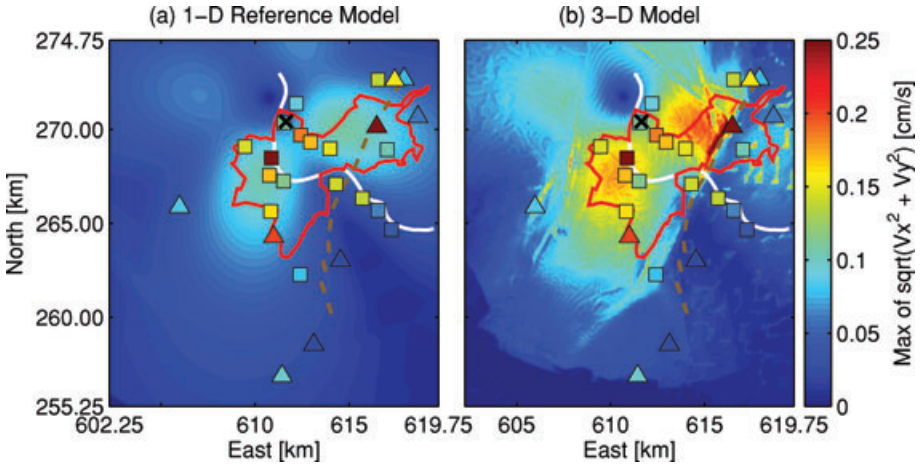

Figure 6. Distributions of horizontal PGV resulting from 3-D simulations. PGV values have been read from the filtered synthetic seismograms. The black 'x' marks the position of the earthquake epicenter. For comparison, colored squares and triangles indicate the horizontal PGV values observed at the permanent and temporary stations, respectively. At station SBAJ (dark red square, PGV = 0.28 cm s^{-1}) and station CHBRI (dark red triangle, PGV = 0.33 cm s^{-1}) the observed PGV exceeds the colorbar limit. Panel (a) displays PGV calculated using the 1-D reference model. The lobes of the source radiation pattern can be seen. Panel (b) presents PGV derived from the synthetics computed for the 3-D model.

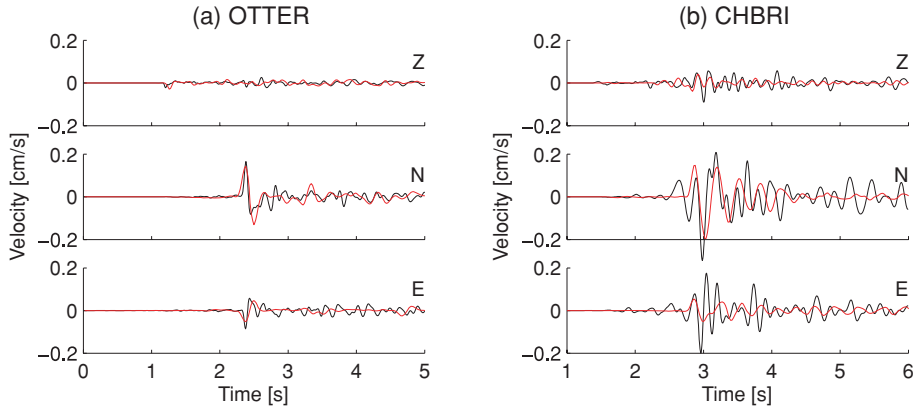

Figure 7. Comparison of recorded (black) and synthetic (red) seismograms at stations OTTER and CHBRI. Traces have been lowpass filtered at 3 Hz (see text for details).

The timing of the first *S*-wave arrival is generally matched within ±0.2 s with the exceptions being stations CHBAL, CHBDO and SRNR, where the arrivals are late by roughly 0.3 s to 0.4 s. Overall, the observed traveltime residuals are non-negligible and they indicate which parts of the geophysical 3-D model require improvements. On the other hand, for studies aiming at an estimate of seismic hazard the timing of the signals is of subordinate importance compared to other characteristics of the seismic waveforms such as the peak ground motions.

One important characteristic of a seismogram that is commonly used for engineering purposes is its response spectrum. We computed spectra for stations OTTER and CHBRI for a damping coefficient of $\zeta = 5$ per cent (Fig. 8). The frequency content of the recorded signals is in most cases satisfactorily reproduced by the synthetic seismograms. In most cases, the match of the spectra even extends for frequencies slightly higher than 3 Hz, before it breaks down for all stations at latest above ∼5 Hz.

The distribution of peak ground velocities of the 3-D simulation using the 3-D model shows significant amplifications in the vicinity of those faults that constitute structural boundaries with pronounced velocity changes across them, in particular close to the main fault at the eastern edge of the basin (Fig. 6b). A similar concentration of high ground motion in narrow zones parallel to major faults has been observed for the $M > 7$ Hyogo-Ken Nanbu earthquake in Kobe, Japan, where a so-called 'damage belt' with a concentration of socio-economic losses was generated (e.g. Kawase 1996).

Whether or not these narrow zones of high ground motion actually occurred during the M_L 3.4 event in Basel cannot be proven because the station distribution is too coarse. One station close to the fault is the temporary station CHBRI, which shows a relatively high PGV value of 1 cm s^{-1} compared to stations closer to the epicenter. However, CHBRI is situated on the eastern side of the fault, which means it is outside the basin, while the strongest amplification is predicted by the simulations on the western side of the fault, that is inside the basin. Furthermore, station CHBRI has on purpose been positioned on very unconsolidated alluvial deposits and the observed high PGV value is therefore likely to be attributed to the amplification of seismic signals by these unconsolidated sediment layers. An interesting set of stations to examine is formed by the LED station WL2 on the eastern side of the fault and WL7 on the western side in about 500 m horizontal distance. There is roughly a factor of two difference between WL7 and WL2 in terms of their horizontal PGV values (0.68 cm s^{-1} versus 0.31 cm s^{-1}), although both of them are positioned on unconsolidated loess sediments. This

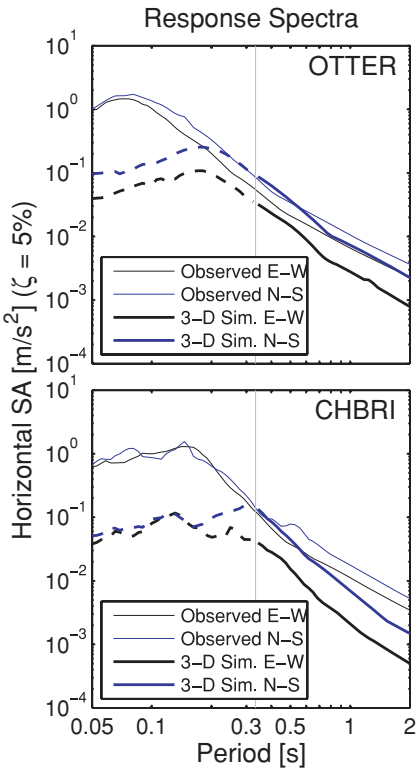

Figure 8. Response spectra at station OTTER and CHBRI. Thin lines represent the spectra of the recorded seismograms, while spectra of the synthetic signals of the 3-D simulation using the 3-D model are plotted as thick lines. The vertical gray line indicates the lower limit of the range of validity of the 3-D simulation. At shorter periods below that limit the synthetic signals consistently underestimate the true amplitudes.

discrepancy could be an indication for the effect of the velocity contrast across the main fault on the pattern of PGV. The concentration of this effect in a narrow zone close to the fault may be the reason why the PGV value at station LOER, another ∼900 m further west of station WL7, is again significantly smaller (0.32 cm s^{-1}). However, an alternative reason for the lower PGV at LOER might be the fact that station LOER is not situated on loess, but rather on the gravels of the lower terraces with somewhat higher Vs velocities (∼400 m s^{-1} compared to ∼160 m s^{-1}, Havenith *et al.* 2007).

4.4.3 Translation of PGV into macroseismic intensities

The spatial distributions of horizontal PGV values obtained by the numerical simulations can be translated into macroseismic intensities using the empirically derived relations developed and calibrated by Kästli & Fäh (2006). However, we have to stress that this conversion is fed with the PGV values of the unfiltered synthetic traces and therefore at least partially operates in a frequency range in which the seismograms may not be accurately modelled. Nevertheless it is worthwhile to perform this conversion for the following reasons: (a) Macroseismic intensity is a very coarse measure and small errors in PGV will not alter the overall intensity distribution much. (b) The response spectra (Section 4.4.2) indicate, that the synthetics exhibit the correct frequency content not only at frequencies below the conservatively estimated limit of 3 Hz, but rather up to about 5 Hz. c) Since the response spectra show that the frequency content at high frequencies is always underestimated by the simulations, the

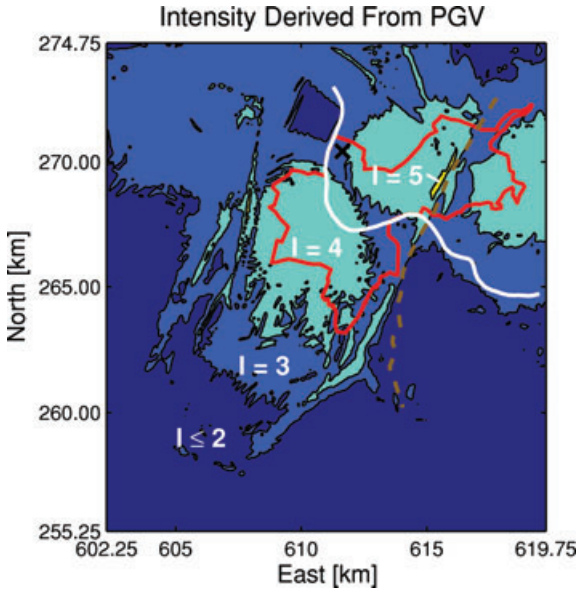

Figure 9. Map of macroseismic intensity derived from PGV values of a 3-D simulation of the M_L 3.4 event. Note that the PGV values have been read from the unfiltered synthetic traces and the intensity values therefore have to be regarded as a lower bound for the intensities. For orientation the map displays the city limits of Basel (red line), the river Rhine (white line) and the approximate position of the main fault on the eastern boundary of the Rhine Graben structure (dashed brown line).

intensity derived from the simulations can at least be seen as a lower bound of the true intensity.

The relations by Kästli & Fäh (2006) are based on the larger PGV of the two horizontal components. They provide intensity values in whole numbers according to the European Macroseismic Scale EMS-98 and they are valid in the range of intensities between II and VII. Fig. 9 displays the obtained distribution of macroseismic intensities for the 3-D simulation of the M_L 3.4 event of 2006 December 8. First of all, the obtained intensity values are of the same order of magnitude as the observed macroseismic intensities. Also the highest observed intensity value of V matches the maximum intensity value predicted by the simulations. Furthermore, the lobes of the source radiation are discernible in the observed macroseismic-intensity distribution. The area with intensity V in our simulation roughly agrees with a zone of intensity V observed in the macroseismic data. On the other hand, the 'hole' with intensity II in the simulated intensity distribution north-west of the epicenter is not visible in the data. We speculate that in the vicinity of the earthquake source the macroseimic observations originate from scattered high-frequency signals which are insufficiently represented in our simulations. It has been consistently observed that the radiation pattern vanishes above a limiting frequency and becomes stochastic in nature (e.g. Castro *et al.* 2006, and references therein).

5 COMPARSION BETWEEN MACROSEISMIC MODEL AND GROUND-MOTION MODEL

Both modelling approaches presented in this study are able to predict the first-order features of the observable effects of an earthquake below the city of Basel. However, in modelling the finer details both models show deviations from each other (Fig. 10), mainly owing to

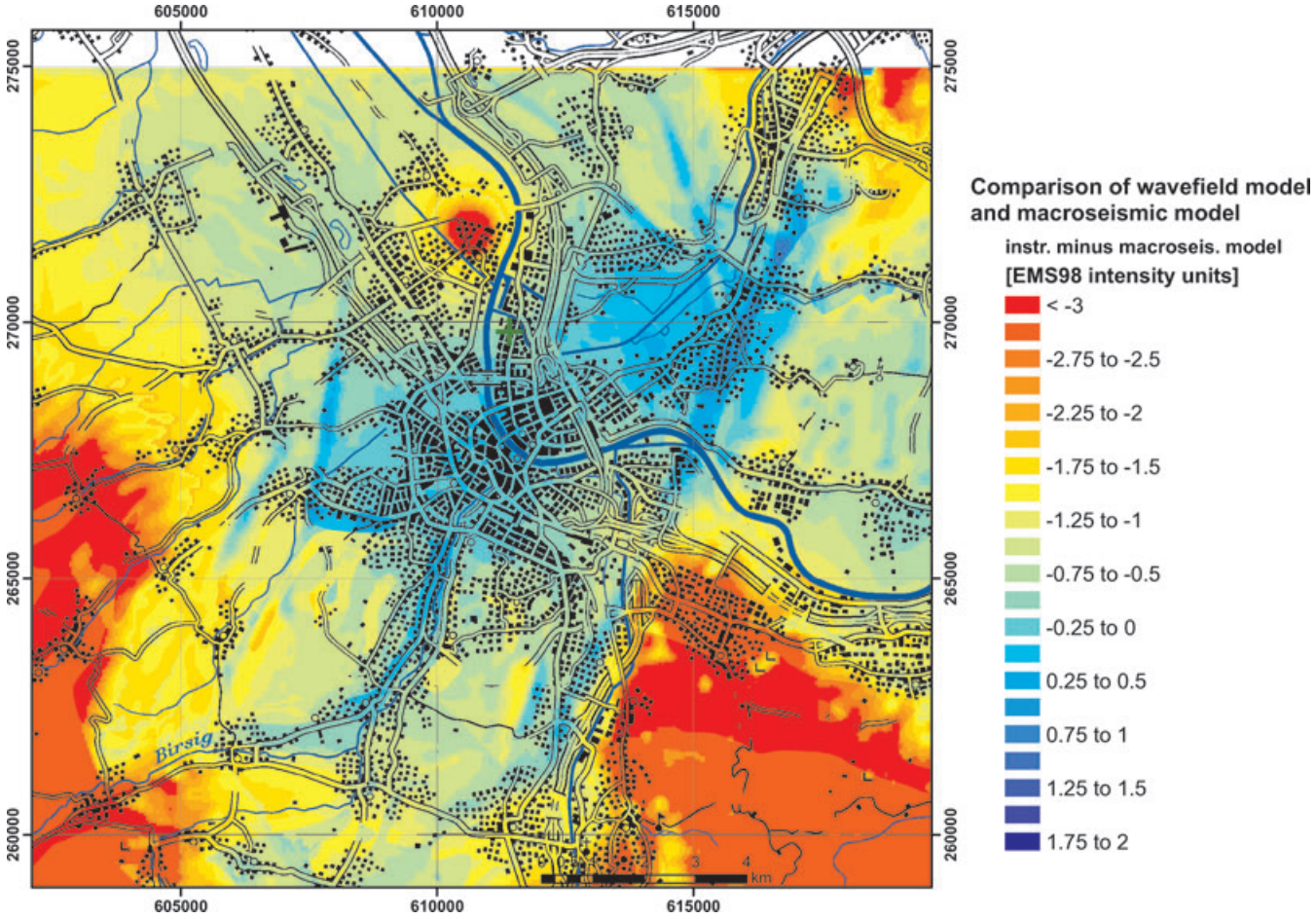

Figure 10. Differences between the intensity values predicted by the macroseismic model and the ground-motion model. Positive values indicate higher intensities predicted by the ground-motion model, negative values indicate higher intensities predicted by the macroseismic model. It has to be kept in mind that the ground-motion model only yields an estimate of the lower bound of intensity (see text for details).

differences in the underlying assumptions and physical processes covered.

In particular, the wave-propagation modelling contains a specification of the focal mechanism and is therefore able to model the source-radiation pattern. This feature would lead to higher predicted intensities in the area covered by the two main lobes of the radiation pattern, comprising most of the city of Basel. However this is counteracted by the fact that the current representation of the 3-D geological structure is too coarse to capture the effects of the uppermost unconsolidated-sediment layers, which in turn are incorporated in the macroseismic model. In combination this leads to a quite consistent model prediction in the city of Basel with models deviating by only about ± 0.5 intensity units. The red spot in Fig. 10 north of Basel (at about 611 000/272 000) is due to the underprediction of intensity by the ground-motion model in this zone, probably because of insufficiently represented scattered high-frequency signals as discussed in Section 4.4.3

The models also disagree in the far-field attenuation of intensity, which shows up at the borders of Fig. 10 where the macroseismic model predicts significantly higher intensities by up to three intensity units. This difference could be due to an incorrect PGV-to-intensity relation, as there are large uncertainties involved in the derivation of such relations, in particular for the low-intensity end of the relation. On the other hand, the attenuation may not be correctly represented in the ground-motion modelling as the Q-factors used in the 3-D structural model are not well constrained.

Finally, to the south-east of Basel, on the eastern side of the main fault the macroseismic model generally predicts higher intensities. This discrepancy probably reflects the fact that the deep 3-D geological structure is not taken into account in the macroseismic model, whereas in the wave-propagation modelling it leads to amplification inside the sedimentary basin (i.e. north-west of the fault) compared to outside of the basin (south-east of the main fault).

6 SCENARIOS FOR A HYPOTHETICAL LARGER EVENT

We use our model tested with the observed $M_L = 3.4$ event to predict the effects of hypothetical events with larger magnitude. The attenuation used for the macroseismic model is calibrated with data of events up to magnitude $M_W = 6.1$ (alpine events) and $M_W = 5.8$ (foreland events). The site amplification values are derived from events with a magnitude range of $M_W = 2.0$ to $M_W = 6.4$. Observed intensities for all calibration data sets range up to VIII according to EMS-98. Therefore, we assume a range of validity for such scenario calculations up to at least $M_W = 5.5$. For larger magnitudes within this range, the site-specific uncertainty resulting from the azimuthal averaging of a point source model will increase. However, based on

expected rupture length and attenuation, the effect of an extended source is still assumed to be below one intensity unit.

The validity of the wave-propagation model in our current approach is limited by our assumption of a double-couple point-source, which is justifiable for small events with a rupture area of several hundred square meters only, but becomes an increasingly severe simplification with increasing size of the earthquake. This limitation could be overcome by specifying extended earthquake sources, but this would add several additional parameters (e.g. rupture direction, rise time, slip distribution) to the model. An investigation of this additional model complexity and the resulting variability in ground motion is beyond the scope of the present study.

In the following we present macroseismic scenarios for a M_W 4.5 and a M_W 5.5 event. For a M_W 4.5 event, the triggering depth of ∼5 km (taking the depth of the main injection well of the geothermal project) may be representative for the whole rupturing process, thus we model it as a shallow event. For a M_W 5.5 event, the rupture size necessitates rupturing rather towards higher depths. For this scenario, we use an intermediate-depth attenuation-model interpolated from the ECOS 'shallow' [5 km] and ECOS 'deep' [12 km] attenuation relations (ECOS: Earthquake catalogue of Switzerland, SED 2002; Fäh *et al.* 2003a).

For an earthquake with magnitude $M_W = 4.5$, we expect macroseismic intensity of VI throughout the entire Basel area including the near Alsace and the German part of the bordering Upper Rhine Graben area. Intensity VII is expected for some isolated localities in the epicentral area. At intensity VII, many well-built ordinary buildings suffer moderate damage; older buildings may show large cracks and failure of fill-walls.

With magnitude $M_W = 5.5$, intensity VII is reached in Basel city and neighboring areas, and some notable damage is unavoidable, reaching intensity VIII in some places. A few well-built ordinary buildings are expected to show serious failures of walls, while weak older structures may collapse. The uncertainty of the presented scenarios is estimated to be about 1 intensity unit, which corresponds in general to the typical uncertainty of singular *a posteriori* intensity assignments. However, the local patterns of the scenarios depend on many factors that are not modelled, such as the effects of the source-radiation pattern and the source directivity. Moreover, local amplifications are very site-specific, depending on factors such as the detailed layer configuration, groundwater table, and subsoil 3-D-structures. While such local information is available at high resolution for Basel city and some adjacent areas from quantitative microzonation studies (Fäh *et al.* 1997; Fäh & Huggenberger 2006), it is missing for large parts of the model space, and therefore it was not included in the models of Figs 11 and 12.

7 CONCLUSIONS

We find that the first-order characteristics of the observations of the M_L 3.4 earthquake of 2006 December 8, in Basel can be well reproduced both by macroseismic models and numerical simulations of seismic wave propagation. These first-order characteristics are the maximum macroseismic intensity reached, the peak ground

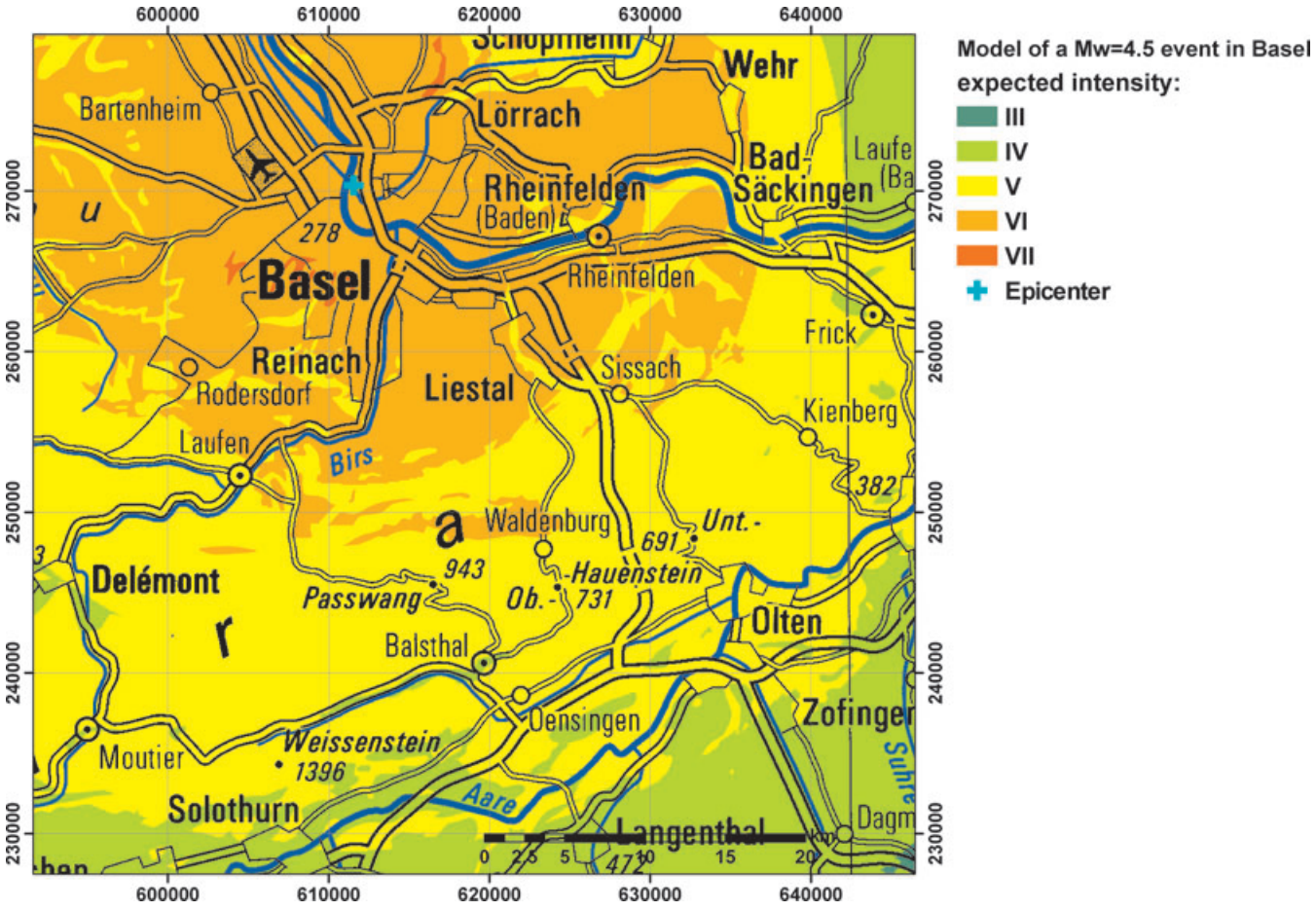

Figure 11. Intensity prediction for a shallow (Depth = 5 km) event with $M_W = 4.5$ and the epicenter at the site of the deep-heat-mining borehole

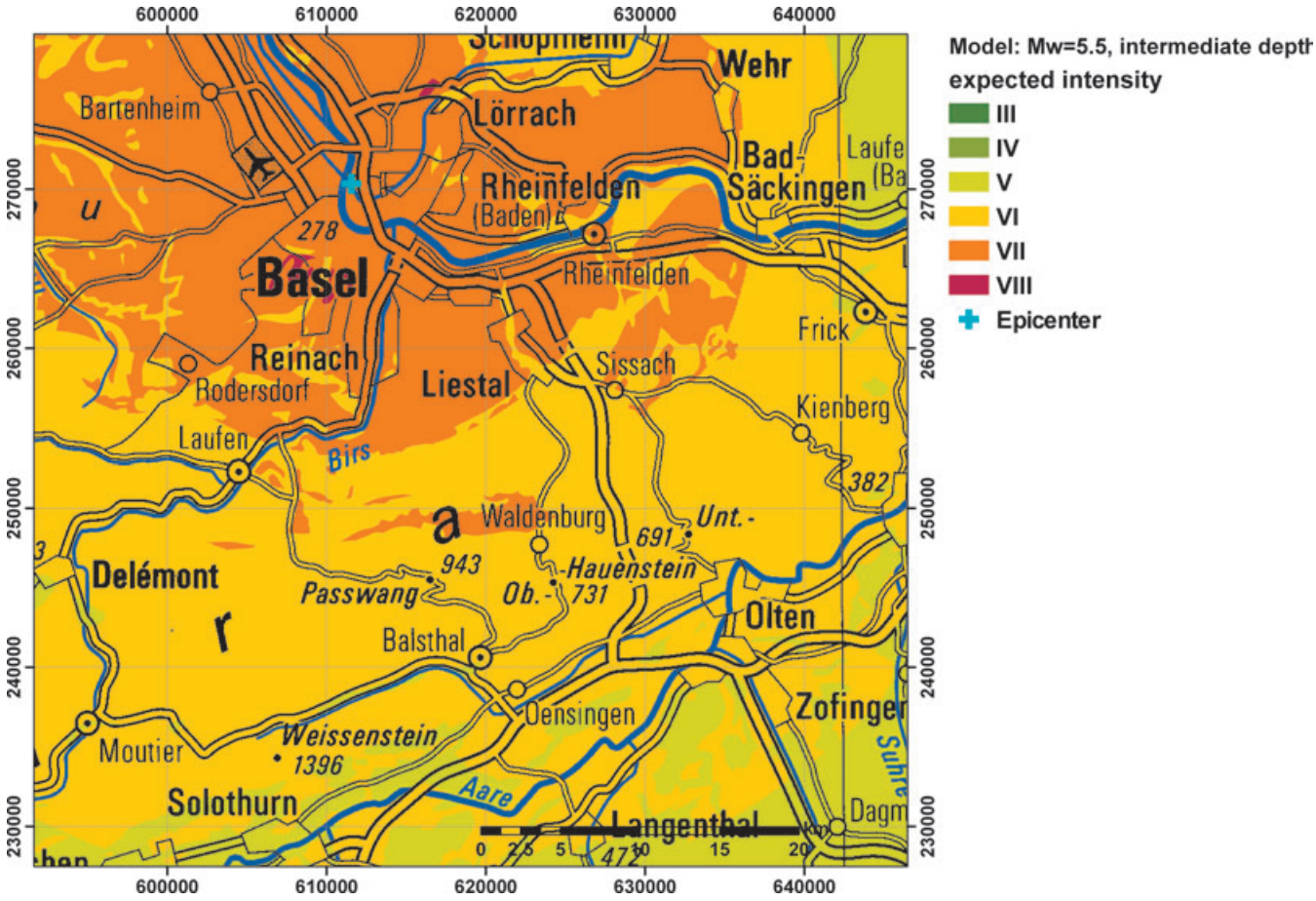

Figure 12. Intensity prediction for an event of intermediate depth with a magnitude $M_W = 5.5$ and the epicenter at the site of the deep-heat-mining borehole.

velocity (within a factor of 2 in most cases, for the filtered seismograms) and the overall intensity distribution. In this sense, nothing particularly 'unusual' can be detected about this event, that is the modelling presented in this paper could have been done before the start of the geothermal reservoir stimulation and one would have had an estimate of the likely effects of an $M_W \sim 3$ event at this location with a reasonable accuracy of ± 1 intensity unit.

A good knowledge of the geophysical 3-D structure of the area has been shown to be the key ingredient for accurate wave propagation simulations. Further development of this model for the wider Basel area by incorporating all available data is one goal of a planned project at the SED.

ACKNOWLEDGMENTS

This study has partially been conducted under a contract with Geopower Basel AG. Part of the work was supported by the project 'Fortsetzungsprojekt Mikrozonierung Region Basel' funded by the Amt für Bevölkerungsschutz Basel-Land and the Sicherheitsdepartement Kanton Basel-Stadt. At these institutions we are grateful to Dr M. Roth and Dr M. Müller for their support of our work. Thanks to Kim Olsen for kindly providing his 3-D finite-difference code AWM. We are also grateful to W. Brüstle and S. Stange at the Landeserdbebendienst Baden-Württemberg for sharing the data of their strong-motion stations. We finally wish to thank the two reviewers for their detailed comments and suggestions which helped to improve the manuscript significantly.

REFERENCES

Aegeter, A. & Bosshardt, O., 2007. Schadenfälle Erdbeben vom 08.12.2006, Tech. Report, Ingenieurbureau A. Aegeter & Dr. O. Bosshardt AG, Basel, available at http://www.geopowerbasel.ch.

Atkinson, G.M. & Kaka, S.I., 2007. Relationships between felt intensity and instrumental ground motion in the Central United States and California, *Bull. seism. Soc. Am.,* **97**(2), 497–510.

Baisch, S., Weidler, R., Vörös, R., Wyborn, D. & de Graaf, L., 2006. Induced seismicity during the stimulation of a geothermal HFR reservoir in the Cooper Basin, Australia, *Bull. seism. Soc. Am.,* **96**(6), 2242–2256.

Bethmann, F., Deichmann, N. & Mai, M., 2007. Moment magnitude, in *Evaluation of the induced seismicity in Basel 2006/2007: Locations, magnitudes, focal mechanisms, statistical forecasts and earthquake scenarios,* Report of the Swiss Seismological Service to Geopower Basel AG, pp. 39–62.

BfL, 2006a. Geologische Karte der Schweiz im Massstab 1:500 000, Vectordata, Bundesamt für Landestopographie, Bern, Switzerland.

BfL, 2006b. Tektonische Karte der Schweiz im Massstab 1:500 000, Vectordata, Bundesamt für Landestopographie, Bern, Switzerland.

Bommer, J.J., Oates, S., Cepeda, J.M., Lindholm, C., Bird, J., Torres, R., Marroquín, G. & Rivas, J., 2006. Control of hazard due to seismicity induced by a hot fractured rock geothermal project, *Eng. Geol.,* **83,** 287–306.

Campus, P. & Fäh, D., 1997. Seismic monitoring of explosions: A method to extract information on the isotropic component of the seismic source, *J. Seismol.,* **1**(3), 205–218.

Castro, R.R., Franceschina, G., Pacor, F., Bindi, D. & Luzi, L., 2006. Analysis of the frequency dependence of the S-wave radiation pattern from local earthquakes in Central Italy, *Bull. seism. Soc. Am.,* **96**(2), 415–426.

Charléty, J., Cuenot, N., Dorbath, L., Dorbath, C., Haessler, H. & Frogneux, M., 2007. Large earthquakes during hydraulic stimulations at the geothermal site of Soultz-sous-Forêts, *Int. J. Rock Mech. Min. Sci.,* **44,** 1091–1105.

Deichmann, N., Ernst, J. & Wöhlbier, S., 2007. Data analysis, in *Evaluation of the induced seismicity in Basel 2006/2007: Locations, magnitudes, focal mechanisms, statistical forecasts and earthquake scenarios,* Report of the Swiss Seismological Service to Geopower Basel AG, pp. 19–38.

Dreger, D., Nadeau, R.M. & Chung, A., 2007. Repeating earthquake finite source models: Strong asperities revealed on the San Andreas Fault, *Geophys. Res. Lett.,* **34**.

Ebel, J.E. & Wald, D.J., 2003. Bayesian estimations of peak ground acceleration and 5% damped spectral acceleration from modified Mercalli intensity data, *Earthq. Spectra,* **19**(3), 511–529.

Fäh, D. & Huggenberger, P., 2006. INTERREG III Erdbebenmikrozonierung am südlichen Oberrhein, Zusammenfassung für das Projekt gebiet in der Schweiz, CD and report (in german; available from the authors), Swiss Seismological Service, ETH Zurich and Kantonsgeologie, University of Basel.

Fäh, D., Rüttener, E., Noack, T.H. & Kruspan, P., 1997. Microzonation of the city of Basel, *J. Seismol.,* **1,** 87–102.

Fäh, D. *et al.*, 2003a. Earthquake Catalogue Of Switzerland (ECOS) and the related macroseismic database, *Eclogae geol. Helv.,* **96,** 219–236.

Fäh, D., Kind, F. & Giardini, D., 2003b. Inversion of local S-wave velocity structures from average H/V ratios, and their use for the estimation of site effects, *J. Seismol.,* **7,** 449–467.

Grünthal, G., 1998. *European Macroseismic Scale 1998,* vol. 15, Cahiers du Centre Européen de Géodynamique et de Séismologie, Centre Européen de Géodynamique et de Séismologie, Luxembourg.

Havenith, H.-B., Fäh, D., Polom, U. & Roulle, A., 2007. S-wave velocity measurements applied to the seismic microzonation of Basel, Upper Rhine Graben, *Geophys. J. Int.,* **170,** 346–358.

Herrmann, R.B., 2004. Computer programs in seismology, Version 3.30, Software package available at http://www.eas.slu.edu/People/RBHerrmann/CPS330.html.

Housner, G.W., 1952. Intensity of ground motion during strong earthquakes, Tech. Report, California Institute of Technology.

Kanamori, H. & Brodsky, E., 2004. The physics of earthquakes, *Rep. Prog. Phys.,* **67,** 1429–1496.

Kästli, P. & Fäh, D., 2006. Rapid estimation of macroseismic effects and shake maps combining macroseismic and instrumental data, in *Proceedings of the First European Conference on Earthquake Engineering and Seismology (ECEES), Geneva, Switzerland, 3–8 September 2006,* CD-ROM.

Kästli, P., Gisler, M. & Fäh, D., 2006. Expert judgment versus automatic and statistical analysis of macroseismic questionnaires, in *Proceedings of the First European Conference on Earthquake Engineering and Seismology (ECEES), Geneva, Switzerland, 3-8 September 2006,* CD-ROM.

Kastrup, U., Zoback, M.L., Deichmann, N., Evans, K.F., Giardini, D. & Michael, A.J., 2004. Stress field variations in the Swiss Alps and the northern Alpine foreland derived from inversion of fault plane solutions, *J. geophys. Res.,* **109,** B01402, doi:10.1029/2003JB002550.

Kawase, H., 1996. The cause of the damage belt in Kobe: "The basin-edge" effect, constructive interference of the direct S-wave with the basin-induced diffracted/Rayleigh waves, *Seis. Res. Lett.,* **67**(5), 25–34.

Kind, F., 2002. Development of microzonation methods: Application to Basel, Switzerland, *Ph.D. thesis*, ETH Zurich, Zurich, Switzerland.

Majer, E.L., Baria, R., Stark, M., Oates, S., Bommer, J., Smith, B. & Asanuma, H., 2007. Induced seismicity associated with Enhanced Geothermal Systems, *Geothermics,* **36,** 185–222.

Margottini, C., Molin, D. & Serva, L., 1992. Intensity versus ground motion—A new approach using Italian data, *Eng. Geol.,* **33**(1), 45–58.

Murphy, J.R. & O'Brien, L.J., 1977. The correlation of peak ground acceleration amplitude with seismic intensity and other physical parameters, *Bull. seism. Soc. Am.,* **67**(3), 877–915.

Olsen, K.B., 1994. Simulation of three-dimensional wave propagation in the Salt Lake basin, Ph.D. thesis, University of Utah, Salt Lake City.

Olsen, K.B., Day, S.M. & Bradley, C.R., 2003. Estimation of Q for long-period (>2s) waves in the Los Angeles basin, *Bull. seism. Soc. Am.,* **93,** 627–638.

Opršal, I., Fäh, D., Mai, P.M. & Giardini, D., 2005. Deterministic earthquake scenario for the Basel area: Simulating strong motions and site effects for Basel, Switzerland, *J. geophys. Res.,* **110,** B04305, doi:1029/2004JB003188.

Schneider-Sliwa, R., Kampschulte, A., Nommel, J.-U., Sandtner, M., Strassmann, R. & Waffenschmidt, C., 1999. Bevölkerungsstruktur und Bevölkerungsdynamik beider Basel, available at http://www.statistik-bs.ch, Statistisches Amt des Kantons Basel-Stadt, Webergasse 34, CH-4005 Basel.

SED, 2002. ECOS—Earthquake catalogue of Switzerland, Tech. Report, Swiss Seismological Service, ETH Zurich, available at www.seismo.ethz.ch.

SED, 2007. Evaluation of the induced seismicity in Basel 2006/2007: Locations, magnitudes, focal mechanisms, statistical forecasts and earthquake scenarios, Report to Geopower Basel AG, Swiss Seismological Service, ETH Zurich.

SIA, 2003. *Einwirkungen auf Tragwerke - SIA Norm 261,* Schweizerischer Ingenieure- und Architektenverband, Zurich, Switzerland.

Spottke, I., Zechner, E. & Huggenberger, P., 2005. The southeastern border of the Upper Rhine Graben: a 3D geological model and its importance for tectonics and groundwater flow, *Int. J. Earth Sci.,* **94,** 580–593.

Wald, D.J., Quitoriano, V., Heaton, T.H. & Kanamori, H., 1999. Relationships between peak ground acceleration, peak ground velocity and Modified Mercalli Intensity in California, *Earthq. Spectra,* **15**(3), 557–564.

Zechner, E., Kind, F., Fäh, D. & Huggenberger, P., 2001. 3-D geological model of the Southern Rhinegraben compiled on existing geological data and geophysical reference modeling, in *Abstract Volume of the 2nd EUCOR-URGENT Workshop, 7–11. October, Mont Saint-Odile,* Strasbourg, France, p. 43.